Comments on "Effect of carbide distribution on the fracture toughness in the transition temperature region of an SA 508 steel"

B. Tanguy, J.Besson, A. Pineau

Ecole des Mines de Paris, Centre des Matériaux, UMR CNRS 7633
BP 87, 91003 Evry Cedex, France

Abstract

Critical cleavage stress values and carbide sizes obtained in a recent work by Lee et al. [1] are recalculated using 2D and 3D FE simulations and new constitutive law, instead of small scale yielding assumption and likely improper choice for the behavior of SA 508 steel. A new model based on the weakest link concept with the determined carbide size distribution (CSD) is succesfully applied to predict K_{Jc} measurements obtained on SA 508 steel and on a similar material (22NiMoCr3-7).

Key words: A. Toughness, B. Statistical model, C. Finite elements analysis.

1 Introduction

This paper comments on a recent publication by Lee et al. [1] on cleavage fracture of SA 508 steel. Following Curry and Knott [2] who showed that the cleavage fracture toughness of a spheroidized steel depends on carbide distribution, most of the models for cleavage fracture of low alloy and mild steels are based on a statistical approach. Contrarily to mild steels, the full characterization of the carbide size distribution in quenched and tempered low alloy steels is difficult to obtain. This is why relevant experimental data are scarcely reported in the literature. In most of the carbide induced cleavage fracture models it is assumed that the carbide size distribution follows an "a priori" function (see e.g. [3,4]).
Recently in a comprehensive study by Lee and al. [1] (hereafter referred to as Lee) the carbide size distribution (CSD) of an SA 508 steel, which is a quenched and tempered low alloy steel, was given based on the analysis of more than 1400 particules. Lee has investigated the effect of carbide distribution on the fracture toughness, K_{Jc}, of this material tested in the lower part of the

transition temperature region where only cleavage fracture occurs without any prior ductile crack growth. Assuming that in this temperature range, cleavage fracture is controlled by a stress criterion and using the maximal principal stress profiles given by McMeeking [5] under plane strain small scale yielding (SSY) conditions, a linear relationship between the critical carbide size initiating cleavage fracture and the test temperature was found. Based on this and on the relationship between the critical nearest–neighbour distance and the CSD, a deterministic relation was proposed between K_{Jc} and the CSD.

However in Lee's work anomalously large values for the critical cleavage stress were reported (see Table 3 in [1]) considering the mechanical properties of this material compared to those obtained on the same steel [3] and in a recent study on a very similar steel [6]. Moreover the SSY assumption for tests carried out on PCVN (Precracked Charpy V–Notch) specimens tested at fracture toughness values as large as 150MPa$\sqrt{\text{m}}$ (see Table 2 in [1]) appears to be strong.

Here, in order to comfort the results obtained by Lee [1], critical cleavage stress values have been recalculated based on the mechanical properties of SA 508 steel and using finite element (FE) calculations. Firstly the SSY assumption was kept in order to check the stress level values reported in Lee's work. Secondly, 3D numerical simulations of PCVN geometry were performed in order to validate the SSY assumption. Then, keeping the Lee's hypothesis that cleavage fracture in quenched and tempered bainitic steels is induced by carbides, and using the CSD obtained on SA 508 steel, a further extension of Lee's work is made to present a statistical model. This model follows the Beremin's formalism [3] but with the CSD given in Lee's work. Model parameters are adjusted to experimental results obtained on SA 508 steel with PCVN geometry and then applied to predict the K_{Jc} values of another quenched and tempered bainitic steel, 22NiMoCr3-7 material which is very close to SA 508.

2 Materials and experiments

Table 1 gives the chemical compositions of the investigated materials. Both were quenched and tempered. Full details can be found in [1].

Material	C	Si	Mn	P	S	Ni	Cr	Cu	Mo	V	Ta	Co	Al
SA 508	0.18	0.1	1.46	0.006	0.003	0.86	0.15	0.03	0.51	0.004	/	/	0.008
22NiMoCr3-7	0.22	0.19	0.89	0.007	0.007	0.87	0.40	0.04	0.55	$< .01$	$< .005$	0.011	0.019

Table 1
Chemical composition of SA 508 and 22NiMoCr3-7 steels (wt.%)

Details on experiments performed on SA 508 steel are given in [1]. Here it is simply reminded that elastic–plastic fracture toughness, K_{Jc}, was determined

using precracked Charpy V–notch (PCVN) specimens ($10 \times 10 \times 55\text{mm}^3$) ($a_0/W \sim 0.5$). Static ($\dot{\varepsilon} = 10^{-3}\text{s}^{-1}$) tensile tests were performed on smooth specimens in 22NiMoCr3-7 material to determine the stress–strain curves at various temperatures. Static plane strain fracture toughness tests were carried out on CT(1T) specimens according to standard ASTM E 1921–97 with a nominal crack length to specimen width ratio (a_0/W) of 0.5. These specimens tested between $-90°\text{C}$ and $-30°\text{C}$ led to pure cleavage fracture.

3 Results

3.1 Tensile properties

The evolution of the yield stress, σ_Y, and ultimate tensile stress, R_m, as a function of temperature is reported in fig. 1a for both steels. The results concerning SA 508 steel are taken from [1]. As shown in fig. 1, σ_Y and R_m are slightly lower for SA 508 steel than for 22NiMoCr3-7 steel. It is worth noting that at a given temperature, the difference between σ_Y and R_m is nearly the same between both steels, which indicates that the hardening capacity for both materials is quite similar over all the investigated temperature range.
The strain hardening exponent, n, in ref. [1], was also given at different temperatures. However, the derivation of the function linking the flow stress and the plastic strain was not given in this paper. Assuming that the usual relation $\sigma_{eq} = K \times \varepsilon^n$ was used by the authors and using the Considère criteria, from which the relation $R_m = K(n/e)^n$ is obtained, it is possible to determine the parameter K at each temperature (the same method was kept at $-196°\text{C}$ where fracture occurred probably before necking) using the tensile properties given for SA 508 steel. Corresponding stress–plastic strain curves obtained at $-196°\text{C}$ and $-100°\text{C}$ are plotted in fig. 1b (thick lines). These curves will be referred to as CL1 model in the following. On the same figure, the experimental stress–plastic strain curve for 22NiMoCr3-7 steel at $-100°\text{C}$ is also plotted. The stress–strain curves for both materials are very close. In the same figure, two other equivalent stress–plastic strain curves are also reported. These curves were obtained using the yield function given by McMeeking [5] (see eq. 1).

$$\left(\frac{\sigma}{\sigma_Y}\right)^{1/N} = \frac{\sigma}{\sigma_Y} + \frac{3E}{2(1+\nu)}\frac{\bar{\varepsilon}_p}{\sigma_Y} \tag{1}$$

Here it is worth mentionning that the McMeeking's FE solutions were used by Lee to obtain the maximum principal stress, σ_{pI}, at each test temperature, and that these values were used to calculate the critical carbide size. This

later point will be discussed in the following. Keeping the n values given in ref. [1] (e.g. $n = N$ in eq. 1), and assuming that the Kirchoff stress tensor can be approximated by the Cauchy stress tensor, leads to much higher stress levels (thin lines on fig. 1b referred to as CL2 model in the following) than stress–strain curves based on SA 508 tensile properties. In particular the ultimate tensile stress inferred from eq. 1 is strongly overestimated at both temperatures. For simplicity's sake, results at other experimental temperatures (-140°C and -75°C) not shown here lead to the same conclusions were drawn.

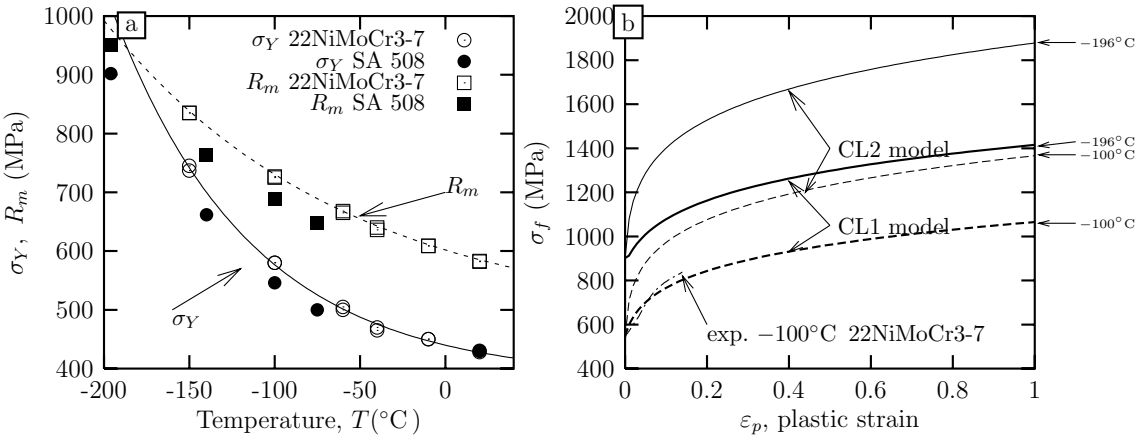

Fig. 1. Evolution of the tensile properties of SA508 and 22NiMoCr3-7 steels as a function of temperature. a) Yield stress and ultimate tensile stress b) Flow stress with CL1 and CL2 models.

3.2 Maximum principal stress, σ_{pI}^{max}, determination

3.2.1 SA 508 steel [1]

In Lee's work the σ_{pI} values at fracture (critical cleavage stress) was presumably obtained at each test temperature by using the McMeeking's FE solutions [5] with CL2 model. Based on the critical stress obtained for 22NiMoCr3-7 and A508 steels with CT(1T) geometry [6], it appears that the stress values indicated in Lee's work are anomalously high, especially when considering that they were obtained with a PCVN geometry [7]. It is reminded that the results presented by McMeeking are based on a SSY assumption, plane strain analysis, and imposing an asymptotic dependence on mode I elastic crack–tip singular field (for more details see [5]). Similar calculations to those presented by McMeeking were made in our study but using the tensile stress–plastic strain curves inferred from the material data given by Lee (labelled CL1).

FE simulations were performed using software Zébulon [8]. Quadratic elements (8 nodes) with reduced integration were used. The boundary layer radii were modified in order to verify SSY conditions varying from 6 mm to 225 mm for K_{Jc} values included between 36.3 and 150 MPa$\sqrt{\text{m}}$.
σ_{pI} profiles corresponding to the experimental K_{Jc} values given by [1] are reported in fig. 2a. This stress reaches a maximum at a distance, X_c. In fig. 2b, the stress profiles corresponding to CL2 model are reported. The maximum values of σ_{pI} for each experimental K_{Jc} value are given in Table. 2 where the values reported by Lee are also given.

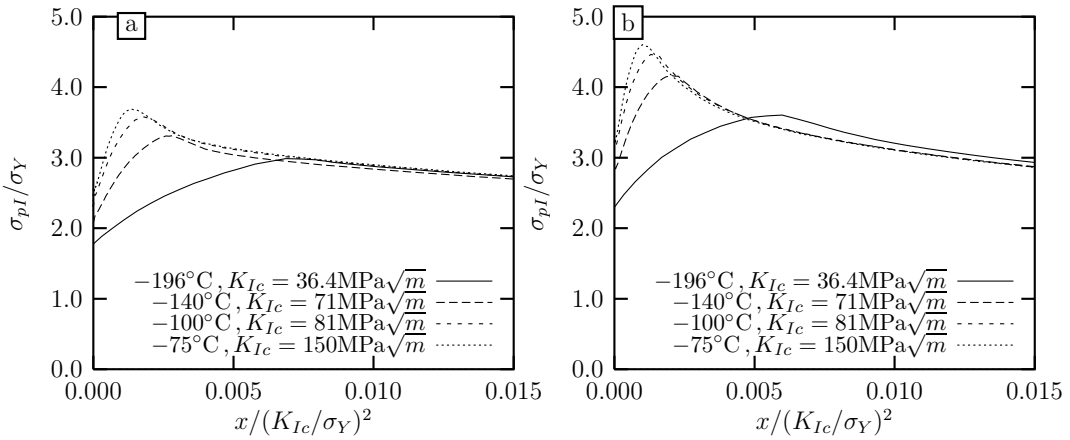

Fig. 2. Maximal principal stress profiles obtained in SSY conditions for SA 508 steel a) with CL1 model b) with CL2 model

From these results, two main conclusions can be drawn : (i) The maximum principal stress, σ_{pI}^{max}, values reported by Lee are much higher than those obtained from simulations with SSY assumption using the stress–strain curves of SA 508 steel (CL1 model). (ii) The σ_{pI}^{max} values reported by Lee are very close to those obtained from simulations with SSY assumption using CL2 model. Similar values are obtained, except at $-196°\text{C}$ were simulations give lower values. From these results it is inferred that the results presented by Lee were obtained using CL2 model as constitutive law for SA 508. Based on fig. 1b, it appears that this hypothesis leads to stress levels much larger than those expected from the material properties. It is then concluded that the σ_{pI}^{max} values reported in Lee's work were largely overestimated, and, that the critical carbide sizes calculated from these values were overly underestimated. Plane strain and full 3D simulations of PCVN specimens were also performed. σ_{pI}^{max} values are reported in Table. 2 while σ_{pI} stress profiles obtained at each test temperatures are shown in fig. 3. It is observed that when the test temperature is higher than $-100°\text{C}$, the SSY assumptions are no longer valid. This result is observed for both plane strain and 3D simulations. Therefore the σ_{pI}^{max} value is lower than that predicted from SSY assumption.

	σ_{pI}^{max} (MPa)			
	$-196°C$	$-140°C$	$-100°C$	$-75°C$
SSY, Lee [1]	3770	2866	2441	2235
SSY + CL1	2694	2192	1954	1844
SSY + CL2	3251	2757	2437	2302
PCVN 3D + CL1	2730	2168	1908	1785

Table 2
Comparison between maximum principal stress values, (σ_{pI}^{max}), obtained with small scale yielding assumption (SSY) and full 3D simulations of PCVN tests using two different constitutive laws (CL1 and CL2).

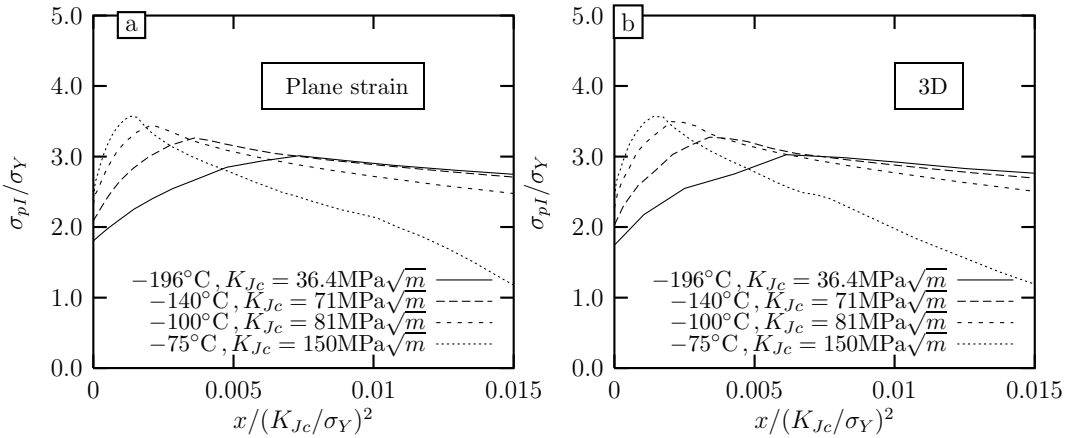

Fig. 3. Principal stress profiles in the mid–section of a PCVN specimen corresponding to the experimental fracture toughness values for SA 508 steel. a) Plane strain b) 3D simulations.

3.2.2 22NiMoCr3-7 steel

In order to determine the σ_{pI}^{max} values corresponding to the K_{Jc} values obtained with this steel, 3D simulations of CT(1T) tests were performed. A good agreement between experimental and simulated load–CMOD curves were obtained at different temperatures. The calculated values of σ_{pI}^{max} are reported in Table 3.

3.3 Determination of the critical parameters

Based on the obtained values for σ_{pI}^{max} and keeping the Lee's assumptions according to which cleavage fracture is stress controlled by the propagation of a microcrack located through the carbides thickness, the critical carbide sizes

was calculated by the authors [1] using a modified Griffith equation given by :

$$d_c = \frac{4E\gamma_p}{\pi(1-\nu^2)(\sigma_{pI}^{max})^2} \tag{2}$$

where γ_p is the effective surface energy (equal to 7 J/m^2 in Lee's work), ν is the Poisson's ratio. The calculated results based on PCVN specimens simulations using the constitutive equation CL1 for SA 508 steel and experimental tensile stress–plastic strain for 22NiMoCr3-7 steel are reported in Table 3. σ_{pI}^{max} values obtained with both plane strain and 3D simulations are reported in Table. 3 for SA 508 steel. These results show that the σ_{pI}^{max} values obtained from 3D simulations are very close to those calculated from plane strain assumption. The evolution of the critical carbide sizes with temperature is reported in fig. 4 where Lee's results are also included. As already indicated by Lee for SA 508 steel, the critical carbide size, d_c, increases linearly with increasing test temperature, but for SA 508 steel the values obtained in the present study are higher due to the lower σ_{pI}^{max} values obtained. Referring to the CSD given by Lee, at the highest test temperature, a very few number of the carbide particles will be eligible to participate to the nucleation of microcracks. Results obtained for 22NiMoCr3-7 steel tested at higher temperature show a weaker temperature dependence of the critical carbide size. However it is observed that at similar temperature (~ -80°C), both materials lead to similar values for the critical size of carbides particles ($\sim 0.7\mu$m), as expected due to the similarity of these materials.

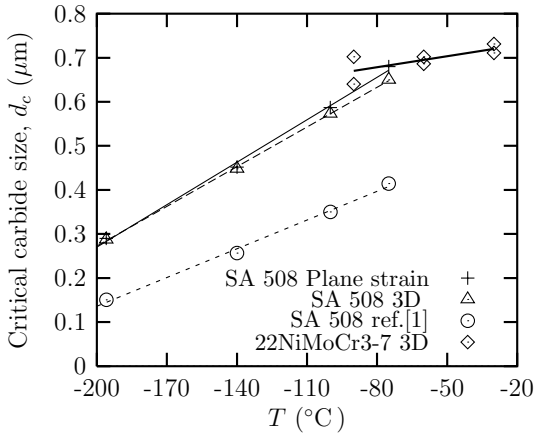

Fig. 4. Critical cardide size (d_c) vs test temperature for SA 508 steel and 22NiMoCr3-7 steel.

4 Statistical model

Lee showed that the probability of finding carbides larger than a given size, d, is given by :

		T (°C)	σ_{pI}^{max}(MPa)	X_c (mm)	d_c (μm)
SA 508	3D (Plane strain)	−196	2730 (2716)	0.0099	0.287
		−140	2168 (2160)	0.038	0.448
		−100	1908 (1885)	0.047	0.573
		−75	1785 (1745)	0.125	0.650
22NiMoCr3-7	Plane strain	−90	1746	0.0148	0.702
		−90	1829	0.0246	0.64
	3D	−60	1740	0.0306	0.702
		−60	1760	0.08	0.686
		−30	1723	0.081	0.711
		−30	1700	0.1021	0.731

Table 3
Maximal principal stress (σ_{pI}^{max}), distance (X_c) from precrack tip to location of maximum principal stress, critical carbide size (d_c).

$$P(size > d) = \exp\left[-\left(\frac{d - d_u}{d_0}\right)^m\right] \tag{3}$$

with d_u=0.00917μm, the size of smallest carbides observed, d_0=0.10158μm and $m = 1.192$, the shape factor of the Weibull distribution.
Assuming that a carbide can lead to the nucleation of a microcrack as soon as plasticity occurs [9], the microcrack size distribution can be represented by the CSD. Fracture occurs when, for a given local stress, σ_{pI}, the carbides size is greater than a critical value, d_c. The value of d_c can be linked to a local fracture toughness, k_{Ic} by the following formula :

$$d_c \sim \frac{1}{\pi}\left(\frac{k_{Ic}}{\sigma_{pI}}\right)^2 \tag{4}$$

Using eq. 3, the corresponding failure probability is :

$$p_r = \exp\left[-\left(\frac{d_c - d_u}{d_0}\right)^m\right] \tag{5}$$

Using a statistical analysis similar to that one proposed by Beremin [3], it can easily be shown that the failure probability is given by :

$$P_R = 1 - \exp\left(-\frac{V}{V_0}\exp\left[-\left(\frac{d_c - d_u}{d_0}\right)^m\right]\right) \tag{6}$$

(where V is the stressed volume) or expressed in terms of stress as :

$$P_R = 1 - \exp\left(-\frac{V}{V_0}\exp\left[-\left(\frac{\frac{1}{\sigma_{pI}^2}-\frac{1}{\sigma_u^2}}{\frac{1}{\sigma_0^2}}\right)^m\right]\right) \quad (7)$$

where $\sigma_0 \sim \frac{1}{\pi^{1/2}}\frac{k_{Ic}}{d_0^{1/2}}$. In Eq. 6, the carbide size threshold, d_u, is equivalent to the introduction of a stress threshold, σ_u, such that $d_u \sim \frac{1}{\pi}\left(\frac{k_{Ic}}{\sigma_u}\right)^2$. This expression leads to $P_R \to 0$ when the stress is close to 0 and to $P_R \to \frac{e^{V/V_0}-1}{e^{V/V_0}}$ when $\sigma_{pI} \to \sigma_u$. For sufficiently large values of V/V_0, P_R tends toward 1.

4.1 Adjustment of the model parameters

Among the four model parameters, σ_u, σ_0, m and V_0, the m value is given by Lee, i.e. $m = 1.192$. It is assumed that this value represents also the CSD for the 22NiMoCr3-7 steel. The reference volume, V_0 is chosen following Beremin's work [3], i.e. as a cubic volume containing about 8 prior austenite grains : $50 \times 50 \times 50\mu\text{m}^3$. Parameters σ_u and σ_0 were fitted to data obtained from PVCN tests on SA 508 steel. Actually only the σ_u parameter has to be fitted on experimental data because it can easily be shown that $\sigma_u/\sigma_0 = (d_0/d_u)^{1/2}$. In SA 508 steel, $\sigma_u/\sigma_0 = 3.328$ was obtained from Lee. In order to investigate the predictive capability of the model the parameter σ_u was determined using SA 508 fracture toughness measured at $-100°\text{C}$ such that a failure probability close to 50% (45%) was obtained for $K_{Jc} = 82.9\text{MPa}\sqrt{\text{m}}$.

5 Results and discussion

Figure 5a shows the evolution of the P_R as a function of the K_{Jc} obtained from the simulations of PCVN tests for SA 508 steel at the test temperatures. In this figure the experimental K_{Jc} values are represented by a full circle. Using the K_{Jc} value at $-100°\text{C}$ to fit σ_u (fig. 5a) leads to $\sigma_u = 14000\text{MPa}$ and $\sigma_0 = 4300\text{MPa}$. In fig. 5a, it is shown that fitting the σ_u parameter at $-100°\text{C}$ tends to high P_R values for the experimental data obtained at lower temperatures. It is clear that testing the applicability of the present model to the results published by Lee [1] would require a set of experimental results much larger than that reported in their publication.
The statistical model was then applied to predict the experimental toughness scattering obtained on 22NiMoCr3-7 steel for which a wider data base was available. The 3D numerical simulations of CT(1T) tests were post–processed in order to evaluate the failure probabilities. For each test temperature, the K_{Jc} values corresponding to P_R= 10%, 50% and 90% are shown in

fig. 5b. Using $\sigma_u = 14000$MPa leads to a good prediction of the experimental scattering at all test temperatures investigated (fig. 5b).

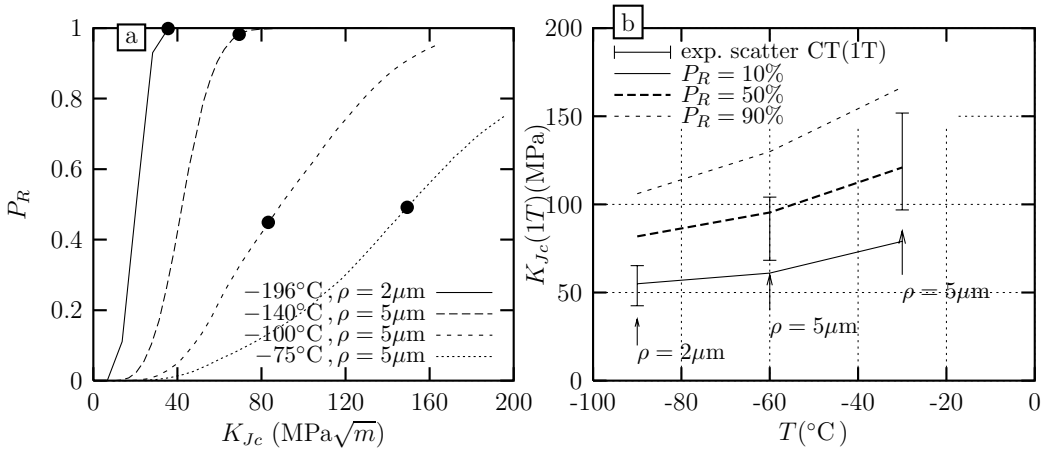

Fig. 5. Evolution of the failure probabilities obtained with the statistical model. a) $\sigma_u = 14000$ MPa fitted on SA 508 results at −100°C on PCVN geometry ($\sigma_0 = 4200$MPa, $n = 1.192$, $V_0 = 0.000125$mm^3) b) Prediction of the fracture toughness scattering on 22NiMoCr3-7 steel with CT(1T) geometry. ρ is the initial mesh crack tip radius.

6 Summary — Conclusions

(1) Anomalously large values for the cleavage stress reported by Lee et al [1] are likely due to two effects in their analysis : (i) the use of a constitutive law for SA 508 steel in Mc Meeking numerical calculations which largely overestimates the stress–strain curves for this material; (ii) the use of plane strain SSY assumption which does not apply when the fracture toughness (i.e. test temperature) is too high.

(2) Lee's results concerning carbide size distribution are used in a new statistical model based on the weakest link concept to predict the variation of fracture toughness with temperature in SA 508 steel.

(3) This model is also applied to another steel (22NIMoCr3-7) for which a larger data base was available, using the CSD measured by Lee. A good agreement between experimental and predicted scattering for the fracture toughness is obtained provided that the parameters appearing in this model are correctly fitted.

References

[1] S. Lee, S. Kim, B. Hwang, B. Lee, C. Lee, Acta Mater. 50 (2002) 4755–4762.

[2] D. Curry, J. Knott, Metal Science (1979) 341–345.

[3] F. Beremin, Met. Trans. 14A (1983) 2277–2287.

[4] Wallin, K. and Saario, T. and Törrönen, K., Metal Science 18 (1984) 13–16.

[5] R. McMeeking, J. Mech. Phys. Solids 25 (1977) 357–381.

[6] B. Tanguy, J. Besson, R. Piques, A. Pineau, in: A. Neimitz, I. Rokach, D. Kocańda, K. Golośi (Eds.), ECF 14 , Fracture Mechanics beyond 2000, Vol. III, EMAS Publishing, Sheffield, 2002.

[7] J. Joyce, R. Tregoning, Eng. Fract. Mech. 68 (2001) 861–894.

[8] J. Besson, R. Foerch, Computer Methods in Applied Mechanics and Engineering 142 (1997) 165–187.

[9] F. Mudry, Nuclear Engineering and Design 105 (1987) 65–76.